HHS Public Access

Author manuscript

Nat Chem. Author manuscript; available in PMC 2020 April 14.

Published in final edited form as:

Nat Chem. 2019 November ; 11(11): 1019–1025. doi:10.1038/s41557-019-0341-7.

Planar three-coordinate iron sulfide in a synthetic [4Fe-3S] cluster with biomimetic reactivity

Daniel E. DeRosha[1], **Vijay G. Chilkuri**[2], **Casey Van Stappen**[3], **Eckhard Bill**[3], **Brandon Q. Mercado**[1], **Serena DeBeer**[3], **Frank Neese**[2], **Patrick L. Holland**[1,*]

[1]Department of Chemistry, Yale University, 225 Prospect Street, New Haven, Connecticut 06520, USA.

[2]Max-Planck-Institut für Kohlenforschung, Kaiser-Wilhelm-Platz 1, D-45470 Mülheim an der Ruhr, Germany.

[3]Max Planck Institute for Chemical Energy Conversion, Stiftstrasse 34-36, D-45470 Mülheim an der Ruhr, Germany.

Abstract

Iron-sulfur clusters are emerging as reactive sites for the reduction of small-molecule substrates. However, the four-coordinate iron sites of typical iron-sulfur clusters rarely react with substrates, implicating three-coordinate iron. This idea is untested because fully sulfide-coordinated three-coordinate iron is unprecedented. Here we report a new type of [4Fe-3S] cluster featuring an iron center with three bonds to sulfides. Although a high-spin electronic configuration is characteristic of other iron-sulfur clusters, the planar geometry and short Fe–S bonds lead to a surprising low-spin electronic configuration at the three-coordinate Fe center as determined by spectroscopy and *ab initio* calculations. In a demonstration of biomimetic reactivity, the [4Fe-3S] cluster reduces hydrazine, a natural substrate of nitrogenase. The product is the first example of NH_2 bound to an iron-sulfur cluster. Our results demonstrate that three-coordinate iron supported by sulfide donors is a plausible precursor to reactivity in iron-sulfur clusters like the FeMoco of nitrogenase.

*Correspondence and requests for materials should be addressed to P.L.H. (patrick.holland@yale.edu).

Author Contributions D.E.D. performed the synthetic experiments, and collected and analyzed spectroscopic data. B.Q.M. and D.E.D. collected and interpreted crystallographic data. C.V.S. and S.D. collected and interpreted the X-ray absorption data. V.G.C. and F.N. performed and interpreted the computational and theoretical aspects. E.B. performed SQUID and magnetic Mössbauer measurements and analyses. P.L.H. supervised the research, and D.E.D. and P.L.H. wrote the manuscript.

Competing Interests The authors declare no competing interests.

Supplementary Information is available in the online version of the paper.

Data availability X-ray crystallographic data have been deposited in the Cambridge Crystallographic Data Centre (http://www.ccdc.cam.ac.uk/) with deposition numbers 1879376 ([4Fe-3S][K]), 1879377 ([4Fe-3S][K]$_2$), 1879378 ([4Fe-3S][K]$_3$), 18793769 ([4Fe-3S][Rb]), 1879380 ([4Fe-3S][Rb]$_2$), 1879381 ([4Fe-3S][Cs]), 1879382 ([4Fe-3S][Cs]$_2$), and 1879383 ([4Fe-3S][K]-NH_2). Copies of the data can be obtained free of charge via https://www.ccdc.cam.ac.uk/structures/. All other characterization data and experimental methods are provided in this article and its Supplementary Information. Data are also available from the corresponding author upon request.

Background

Iron-sulfur clusters are best known for electron transfer[1], and chemists' current understanding has benefitted from synthetic models[2,3,4]. Resting state structures of iron-sulfur clusters provide a natural starting point for synthetic modeling, and the most common structural elements are the [4Fe-4S] cubane and [2Fe-2S] diamond shapes. Recent advances include the isolation of all-ferrous[5] and all-ferric[6] [4Fe-4S] cubanes, preparation of a diferrous [2Fe-2S] cluster[7], and isolation of several higher nuclearity [8Fe-9S] double cubanes with shapes reminiscent of the nitrogenase iron-molybdenum cofactor in its resting state[8,9]. However, iron-sulfur clusters are dynamic and can undergo structural rearrangements to facilitate substrate binding and stabilize reactive intermediates[10], as highlighted by reversible rearrangements of the cofactors of CODH and hydrogenase enzymes[11,12,13]. In catalytically relevant examples of cluster flexibility, three-coordinate Fe in an all-sulfide environment has been postulated to enable cluster reactions, as in biotin synthase where the substrate *S*-adenosylmethionine coordinates to an iron atom supported by three sulfides[14]. Despite this emerging picture of iron-sulfur clusters as flexible assemblies, known synthetic iron-sulfur clusters have iron sites that are four-coordinate and tetrahedral like the biological resting state structures, which limits our understanding of the unsaturated active forms that may be essential for reactivity. Accordingly, few substrate reductions by iron-sulfur clusters are known[15,16,17,18]. Three-coordinate species (potentially accessible from cleavage of weak iron-sulfide bonds) are expected to be quite active based on the reactivity of low-coordinate molecular Fe complexes[19], making them compelling targets.

A salient example is nitrogenase[20], in which the crystallographically characterized FeMoco and FeVco active sites orchestrate the challenging conversion of dinitrogen into ammonia[20]. Four-coordinate belt Fe atoms in the FeMoco (Fig. 1a) and FeVco cofactors, which are connected to three sulfide ligands (S^{2-}) and an interstitial carbide ligand (C^{4-}) in the resting state[21,22], have been shown to undergo Fe–S bond cleavage[23,24]. The point in the mechanism at which bonds break, and the structure of the activated form that binds substrate, are unclear. Moreover, to our knowledge there is no experimental precedent for binding of dinitrogen reduction intermediates (N_xH_y: x = 1, 2; y = 0–5) to any synthetic iron-sulfur cluster. Three-coordinate iron in a cluster may therefore provide insight into the properties that are accessible in iron-sulfur clusters, and also address the chemistry underlying substrate binding by nitrogenase.

Results and Discussion

Synthesis and Structures of [4Fe-3S] Clusters

In this work, we report a new series of clusters supported by diketiminate ligands, which are adept at stabilizing low-coordinate metal sites in coordination complexes[19]. Previous work has demonstrated diketiminate-supported diiron sulfide complexes[25,26]; however, in these prior examples, the iron sites each contain some biologically non-relevant N-based donors. We hypothesized that use of a smaller diketiminate framework (see ligand in Fig. 1b) might enable formation of higher nuclearity clusters while maintaining low coordination numbers. Using the previously reported iron(I) complex $L^{Me}Fe(C_6H_6)$[27] (L^{Me} = 2,3,4-trimethyl-2,4-

bis(2,6-dimethylphenyl)iminopent-3-yl) we found that reduction with KC_8 followed by addition of the S-atom transfer reagent $SPMe_3$ at low temperature resulted in formation of a single major product, as judged by ^1H NMR spectroscopy (Fig. 1b), which could be isolated in 65% yield. Single crystal X-ray diffraction revealed the structure to be a tetranuclear [4Fe-3S] iron sulfur cluster (**1**) with three bridging sulfides that connect three iron-diketiminate fragments in a hexagonal arrangement (Fig. 1c). A fourth Fe atom is ligated only by three sulfide ligands, and is planar (sum of angles at Fe = 360 ± 0.5°). There are also two potassium cations located above and below the plane of the cluster. The connectivity of the [4Fe-3S] core was further established by the synthesis and structural characterization of analogues of **1** with Rb and Cs countercations (described in the Supplementary Material).

The [4Fe-3S] cluster **1** is the first example of an iron-sulfur cluster that contains a three-coordinate iron site in an all-sulfide environment, providing a unique opportunity to learn about the properties of iron with one fewer sulfide ligands than found in previous clusters. We briefly compare the core of **1** to other clusters, including the FeMoco (Fig. 2). The majority of known four iron-sulfur clusters are [4Fe-4S] cubanes; to date, the most reduced biological clusters have all Fe^{2+} ions[15,28], while synthetic nitrosyl-bound cubanes have been reported with formal oxidation states of less than +2 per iron[29,30]. The new [4Fe-3S] cluster **1** formally contains three Fe^{2+} sites and one Fe^{1+} site, making it among the most reduced tetranuclear iron-sulfur clusters. The peripheral Fe–S bonds in **1** of 2.34 ± 0.01 Å are similar in length to the all-Fe^{2+} cubane of the [4Fe-4S] iron protein in nitrogenase (average Fe–S bond lengths of 2.33 ± 0.05 Å[28]), and are within error of those reported in a synthetic cubane at the all-ferrous oxidation level (2.33 ± 0.05 Å)[5].

The average Fe–S lengths to the central three-coordinate iron in **1** (2.17 ± 0.01 Å), on the other hand, are significantly shorter than average Fe–S bonds in [4Fe-4S] clusters (2.29 ± 0.04 Å)[31], but within error of the Fe–S bond in a three-coordinate diketiminate-supported diiron(I) system with only one sulfide donor (2.174 ± 0.006 Å)[26]. Similarly short Fe–S bonds have been observed at tetrahedral sulfide-supported Fe in “ladder” type [3Fe-4S] clusters (average Fe–S of 2.193 ± 0.07 Å)[32] as well as in a hexanuclear [6Fe-S5] cluster (average Fe–S of 2.20 ± 0.01 Å in a $Fe_4(\mu_2\text{-}S)_2$ core)[33]. The short Fe–S bond distances to the central three-coordinate iron in **1** are also reminiscent of those to the belt Fe sites in the FeMoco (average Fe6–S bond length is 2.20 Å; Fig. 2b)[22]. The geometry of the central Fe site resembles the one in a three-coordinate Fe^{2+} tris(thiolate) complex reported by Power, which exhibits a planar coordination environment (sum of angles at Fe = 359.9 ± 0.2), but the Fe–S bonds at the tris(thiolate) site are 0.1 Å longer than those in **1** (average Fe–S of 2.274 ± 0.005 Å)[34]. Although there is no precedent for planar iron-sulfide clusters with more than two Fe atoms, a planar arrangement similar to the central site in **1** has been proposed within a potential intermediate state of the FeMoco[20]. Attainment of this planar geometry would require dissociation of the central carbide from the FeMoco resting state, in which the distorted tetrahedral geometry at Fe6 (τ = 0.88[35]) leads to a 0.47 Å separation between Fe6 and the plane defined by three sulfide ligands.

The cyclic voltammogram (CV) of **1** in THF solution with 0.2 M tetrabutylammonium hexafluorophosphate electrolyte exhibits a reversible reduction at −3.14 V versus ferrocene (Supplementary Fig. 44), and addition of one molar equivalent of the strong reductant KC_8

led to the formation of one-electron reduced **2**. X-ray crystallography shows that the [4Fe-3S] core is retained in **2**, and an additional potassium cation interacts with the aryl group of a diketiminate supporting ligand (Fig. 1c). Cluster **2** formally contains two Fe^{1+} sites and two Fe^{2+} sites, and is unstable in solution ($t_{1/2}$ = 20 min by UV-vis spectroscopy; see Supplementary Fig. 47–48), which prevented more thorough characterization. The CV of **1** also shows an irreversible oxidation at −1.89 V, and use of KBArF electrolyte (BArF = tetrakis[3,5-bis(trifluoromethyl)phenyl]borate) results in a quasi-reversible wave at −2.05 V (see Supplementary Fig. 44). Oxidation with one molar equivalent of $AgPF_6$ forms a new product **3** in 77% isolated yield. X-ray crystallography reveals **3** to be a more oxidized all-Fe^{2+} cluster in which one of the two potassium cations present in starting material **1** is absent (Fig. 1c). Overall, the [4Fe-3S] core is retained across three oxidation levels, with minor structural perturbations accompanying these changes in cluster oxidation level (see Supplementary Fig. 50–51 for structural comparisons of **1–3**). The minor structural change across oxidation states is reminiscent of the [4Fe-4S] iron protein in nitrogenase, which also undergoes little reorganization over three oxidation levels[28].

Spectroscopic and Computational Studies

The physical oxidation states of the Fe atoms in the different oxidation levels of the [4Fe-3S] clusters were characterized using iron K-edge X-ray absorption spectroscopy (XAS). Analysis of three- and four-coordinate Fe^{2+} reference compounds in addition to clusters **1**, **3**, and **4** (a more oxidized cluster described below) revealed a clear trend in the near edge region of the XAS data (Fig. 3a and Supplementary Fig. 40). We assign a shoulder at ~7115 eV to a $1s \rightarrow 4p_z$ transition at the central trigonal-planar iron atom (see discussion in the Supplementary Material), which shifts to higher energy by 0.41 eV going from Fe^{1+} containing **1** to all-ferrous **3**. These data are consistent with oxidation of the central iron atom.

We evaluated the electronic structures of **1** and **3** using Mössbauer spectroscopy, electron paramagnetic resonance (EPR) spectroscopy, and *ab initio* calculations. We first discuss cluster **3**, which has all Fe^{2+} sites and accordingly displays a featureless perpendicular mode EPR spectrum. Its Mössbauer spectrum (Fig. 3c) is a superposition of two doublets in a 3:1 ratio that correlates to the outside and inside Fe sites. The smaller subspectrum (assigned to the central Fe^{2+} site) has an isomer shift of 0.37 mm/s that is far outside the range reported for Fe^{2+} sites in previously reported iron-sulfur clusters (0.6–0.8 mm/s)[5,7,36,37]. Instead, this low isomer shift is characteristic of low-spin Fe^{2+} sites[38], which is surprising to find in the presence of three (normally) weak-field sulfide ligands. The low-spin d^6 assignment is corroborated by the negligible quadrupole splitting observed for the Mössbauer signal for the central iron, and confirmed by variable-field Mössbauer spectra of **3** that reveal the central iron to be diamagnetic (Supplementary Fig. 68). Mössbauer spectra of the Rb and Cs analogues are almost identical to that of **3** (see Supplementary Fig. 35 and Supplementary Fig. 37).

Wavefunction based *ab initio* calculations at the complete active space self-consistent field (CASSCF) and N-electron valence-perturbation theory (NEVPT2) levels were carried out. In order to use the *ab initio* ligand theory (AILFT) method[39] for insight into the local ligand

fields of each individual Fe^{2+} site in **3**, we constructed four models of **3** where all but one of the Fe^{2+} ions were replaced with Zn^{2+} ions. This isolates the change in the ligand-field characteristics of each iron site. The calculations suggest two reasons for the surprising low-spin configuration at the planar Fe^{2+} site (Fe4). First, the very short Fe–S bonds to the central Fe4 (right of Fig. 4, in red) cause the near-degenerate d_{xy} and d_{x2-y2} orbitals to be 6,000 cm^{-1} higher in energy than the next set of orbitals (d_{xz} and d_{yz}), a splitting that is much larger than usual tetrahedral sites in iron-sulfur clusters (and the outer sites in **1**–**3**), which have ligand-field splittings of ~3,500 cm^{-1} [40]. Second, the high covalency of the Fe–S bonds gives a reduction in the Racah B parameter,[41] which is calculated to be 6–8% lower at the central Fe than the outer sites. This decrease in electron-electron repulsion also contributes to a preference for a low-spin electronic configuration, in which these two high-lying orbitals are unoccupied.

The reduced complex **1** has three Fe^{2+} ions and one Fe^{1+} ion, and is a rare example of Fe^{1+} bound to sulfide[26,42]. At 10 K in a toluene glass, **1** exhibits a nearly axial EPR spectrum near g_{eff} = 2 (Supplementary Fig. 38), which indicates an S = 1/2 ground state from antiferromagnetic coupling between the four paramagnetic iron centers. We sought to determine the location of the ‘extra’ electron in this reduced mixed-valent cluster. At 80 K, zero-field Mössbauer measurements of powder samples of **1** show three quadrupole doublets in a 2:1:1 ratio (Fig. 3b). DFT calculations gave Mössbauer parameters that agree with the experimental spectrum within 0.10 mm/s only when the central iron site is assigned as Fe^{1+} (see Supplementary Table 4 and Supplementary Fig. 59). This assignment also agrees with the XAS data described above. There are only two previous examples of Fe^{1+} bound to sulfide: one with a phosphorus-based supporting ligand and low-spin iron(I)[42], and one with a nitrogen-based supporting ligand and high-spin iron(I)[26]. In **1**, the isomer shift of the central iron (0.34 mm/s) is closer to the low-spin Fe^{1+} precedent (0.22 mm/s) than the high-spin precedent (0.67 mm/s), suggesting that **1** also has low-spin Fe^{1+}. In addition, the isomer shift of this site is very similar to that in the central site of **3**, which is low-spin as discussed above. However, given the empirical nature of this evidence and the few precedents, our conclusions regarding the spin state at the Fe^{1+} site in **1** should be considered tentative. The outer three iron sites are high-spin Fe^{2+}, as shown by their nearly identical isomer shifts and excellent agreement with other tetrahedral ferrous ions bound to sulfide and nitrogen atom donors (~0.8 mm/s)[7,37]. One of the outer Fe^{2+} sites in **1** has a different quadrupole splitting because of a twisting of its geometry as observed in the X-ray crystal structure (Supplementary Fig. 55). Mössbauer spectra of different alkali-metal analogues show that the quadrupole splitting of the outer Fe sites has a small but systematic variation with the twist angle, decreasing in the order K>Rb>Cs (see Supplementary Fig. 56 for details).

Upon reduction of [4Fe-3S] cluster **2** to form **1,** the ligand field at the central Fe4 site is perturbed as expected for a low-spin iron(I) ion with high-lying near-degenerate d_{xy} and d_{x2-y2} orbitals. As shown in Supplementary Fig. 61, the energy gap between the d_{xy} and d_{x2-y2} orbitals at the central Fe^{1+} site in **1** is ~500 cm^{-1}, compared to only ~51 cm^{-1} in the all-Fe^{2+} cluster (**3**). This splitting is consistent with the expected Jahn-Teller distortion of a low-spin iron(I) complex (see SI for details).

Thus, the new type of planar three-coordinate Fe site in clusters **1** and **3** has two distinctive spectroscopic signatures: a pronounced pre-edge feature at 7115 eV that corresponds to an unusually low energy $1s \rightarrow 4p_z$ transition, and a Mössbauer signal with a low isomer shift of 0.36 ± 0.02 mm/s. This low isomer shift is seen in the three-coordinate all-sulfide site in both oxidation levels, and with a variety of alkali metal capping cations. We suggest that these spectroscopic signatures could help to identify unsaturated sites in intermediate states of enzymes like nitrogenases and that the low-spin configuration should be sought in unsaturated sites in natural iron-sulfur clusters.

Reactivity with N–N Bonds

The presence of an unsaturated three-coordinate iron site in **1**–**3** prompted us to explore the reactivity of these clusters with small molecules relevant to nitrogenase. We observed that the reaction of **3** with 0.5 molar equivalent of the nitrogenase substrate hydrazine (N_2H_4) results in rapid and near-quantitative (80% spectroscopic yield) formation of a new product with C_{3v} symmetry, as judged by ^{1}H NMR analysis (Fig. 5a). This new product (**4**) gave purple-red crystals for which diffraction reveals a [4Fe-3S] cluster in which a new N-based ligand is bound to the central iron (Fig. 5b). It was possible to identify this ligand as amide (NH_2) through IR and ^{1}H NMR spectroscopies (Fig. 5d). The IR spectrum of crystalline **4** shows two N–H stretching vibrations at 3262 and 3352 cm^{-1}, which shift to 2499 and 2372 cm^{-1} when **4** is synthesized from N_2D_4 (Supplementary Fig. 26). The ^{1}H NMR spectrum of **4** can be fully assigned based on integrations of the various paramagnetically shifted signals, and the peak corresponding to the NH_2 protons is absent when deuterated **4** is measured (Fig. 5d). The identity of the NH_2 ligand was also verified by treating **4** with excess HCl, which produced 0.81 equiv of NH_3 per equiv of **4**. Amide **4** can be independently synthesized using Carpino's hydrazine[43] (see Supplementary Material for details) which demonstrates its utility as an amido transfer reagent.

The rapid reaction of **3** with N_2H_4 shows that this all-Fe^{2+} cluster can break an N–N bond, and it is significant that we have observed a hydrazine-derived NH_2 group on an iron-sulfur cluster for the first time. Despite their implication in late-stage nitrogen reduction by the FeMoco[20], there are only three previously reported terminal iron amide (Fe–NH_2) complexes, none of which are iron-sulfur clusters, and none of which derive from precursors with N–N bonds[44,45,46]. However, Szymczak recently reported a bridging iron amide formed from hydrazine[47]. The Fe–N bond distance in **4** is 2.06 ± 0.02 Å, which lies in the range of previous parent amido iron complexes (1.918 ± 0.003 to 2.069 ± 0.007 Å)[44,45,46]. The most salient difference between the molecular structure of **4** and the [4Fe-3S] clusters **1**–**3** is a change in geometry of the central Fe from trigonal planar to distorted tetrahedral, in which the central Fe is raised 0.9 Å out of the plane defined by the six peripheral iron and sulfur atoms (Supplementary Fig. 54).

Compound **4** formally contains three Fe^{2+} ions and one Fe^{3+} ion. The zero-field Mössbauer spectrum of **4** at 80 K has two strongly overlapping quadrupole doublets in a 3:1 ratio, with isomer shifts of 0.76 and 0.74 mm/s, respectively (Fig. 5c). While the 3:1 ratio could be taken to imply that the Fe^{3+} site is the central NH_2-bound iron, its isomer shift is inconsistent with previous four-coordinate Fe^{3+} sulfide sites (~0.3 mm/s)[6,48]. Therefore, we

suggest that the hole is delocalized over the three peripheral Fe sites, with averaged oxidation states of +2.33, while the central iron is high-spin Fe^{2+}. Consistent with this assignment, the Fe–S bond distances at the central Fe (avg. 2.297 ± 0.002 Å) are similar to those in another four-coordinate high-spin Fe^{2+} site supported by three sulfide donors and a carbene ligand (2.33 ± 0.002 Å)[5].

Consistent with the proposal that sulfide-supported Fe^{2+} in the key substrate binding intermediate of the FeMoco performs substrate reductions[24,49], our results demonstrate that Fe^{2+} in **3** is sufficiently reduced to cleave the N-N bond in hydrazine, and suggest that Fe^{2+} is an appropriate oxidation state to target in reactive iron-sulfur clusters. Additionally, reduction of hydrazine with **3** with to form NH_2-bound **4** is relevant to substrate reduction by the FeMoco. Rapid freeze-trapping during nitrogenase turnover with hydrazine, diazene, and methyldiazene has revealed a common intermediate with a single N environment by EPR and ENDOR[50,51]. This species has been proposed to be either an NH_x species or a highly symmetric hydrazine adduct. Reaction of our [4Fe-3S] model system with N_2H_4 to form NH_2 therefore supports the feasibility of the former proposal for the FeMoco. The approach here uses a synthetic iron-sulfur cluster in which the reactive Fe site is supported exclusively by sulfide, which is an important step beyond molecular Fe complexes supported by non-biologically relevant N, P, and B coordinated supporting ligands that have previously furnished N_2 reduction intermediates[52,53,54]. Cluster **4** provides the first precedent for binding of an N_xH_y intermediate to a synthetic iron-sulfur cluster. Though we have not observed reactions of **1–3** with N_2, we anticipate that future variation of the ligand, countercation, or oxidation state will enable this more difficult reduction.

Conclusion

Using diketiminate supporting ligands, it is possible to isolate a stable iron-sulfur cluster that has all-sulfide coordination at a planar three-coordinate iron site. The [4Fe-3S] clusters reported here show that lowering the coordination number of iron can cause a surprising change to a low-spin electronic configuration, which is the result of short, highly covalent in-plane Fe–S bonds that lead to strong ligand-field splitting. The unusual geometry leads to XAS and Mössbauer signatures that may help to identify trigonal-planar sites in biological clusters. In addition, we show that this new type of low-coordinate site can reduce N_2H_4, in an example of biomimetic N–N reduction. More generally, these findings demonstrate the utility of targeting intermediate structures, in addition to enzymatic resting states, as a strategy to realize biologically relevant reactivity through synthetic modeling.

Supplementary Material

Refer to Web version on PubMed Central for supplementary material.

Acknowledgments

This work was supported by the National Institutes of Health (GM065313 to P.L.H.), the Max Planck Society (E.B., S.D.B. and F.N.), and IMPRS-RECHARGE (C.V.S.). We thank Andreas Göbels for measurement of SQUID data, and Gary Brudvig, Gourab Banerjee, Daniel Suess, and Amy Speelman for help with EPR spectroscopy. We thank Christopher Cummins and Wesley Transue for insightful conversations and the gift of Carpino's hydrazine. Elemental analysis data were measured at the CENTC Elemental Analysis Facility at the University of Rochester,

funded by the NSF (CHE-0650456), and we thank William Brennessel for collecting these data. XAS spectra were measured at SSRL 9–3 and ESRF ID-26, and we thank Matthew Latimer and Blanka Detlefs for their assistance during measurements. Use of SSRL is supported by the DOE, BES (DE-AC02–76SF00515). The SSRL SMB program is supported by DOE, BER and NIH (including P41GM103393).

References

1. Beinert H, Holm RH & Munck E Iron-sulfur clusters: nature's modular, multipurpose structures. Science 277, 653–659 (1997). [PubMed: 9235882]
2. Lee SC, Lo W & Holm RH Developments in the biomimetic chemistry of cubane-type and higher nuclearity iron-sulfur clusters. Chem. Rev 114, 3579–3600 (2014). [PubMed: 24410527]
3. Venkateswara Rao P & Holm RH Synthetic analogues of the active sites of iron−sulfur proteins. Chem. Rev 104, 527–560 (2004). [PubMed: 14871134]
4. Bill E Iron-sulfur clusters - new features in enzymes and synthetic models. Hyperfine Interact. 205, 139–147 (2012).
5. Deng L & Holm RH Stabilization of fully reduced iron−sulfur clusters by carbene ligation: the [FenSn]0 oxidation levels (n = 4, 8). J. Am. Chem. Soc 130, 9878–9886 (2008). [PubMed: 18593124]
6. Moula G, Matsumoto T, Miehlich ME, Meyer K & Tatsumi K Synthesis of an all-ferric cuboidal iron–sulfur cluster [FeIII4S4(SAr)4]. Angew. Chem. Int. Ed 57, 11594–11597 (2018).
7. Albers A, Demeshko S, Pröpper K, Dechert S, Bill E & Meyer F A super-reduced diferrous [2Fe–2S] cluster. J. Am. Chem. Soc 135, 1704–1707 (2013). [PubMed: 23320988]
8. Ohki Y, Ikagawa Y & Tatsumi K Synthesis of new [8Fe-7S] clusters: a topological link between the core structures of P-cluster, FeMo-co, and FeFe-co of nitrogenases. J. Am. Chem. Soc 129, 10457–10465 (2007). [PubMed: 17676736]
9. Zhang YG & Holm RH Synthesis of a molecular Mo2Fe6S9 cluster with the topology of the P-N cluster of nitrogenase by rearrangement of an edge-bridged Mo2Fe6S8 double cubane. J. Am. Chem. Soc 125, 3910–3920 (2003). [PubMed: 12656626]
10. Holm RH & Lo W Structural conversions of synthetic and protein-bound iron–sulfur clusters. Chem. Rev 116, 13685–13713 (2016). [PubMed: 27933770]
11. Wittenborn EC, Merrouch M, Ueda C, Fradale L, Léger C, Fourmond V, Pandelia M-E, Dementin S & Drennan CL Redox-dependent rearrangements of the NiFeS cluster of carbon monoxide dehydrogenase. eLife 7, e39451 (2018). [PubMed: 30277213]
12. Fritsch J, Scheerer P, Frielingsdorf S, Kroschinsky S, Friedrich B, Lenz O & Spahn CMT The crystal structure of an oxygen-tolerant hydrogenase uncovers a novel iron-sulphur centre. Nature 479, 249–252 (2011). [PubMed: 22002606]
13. Shomura Y, Yoon K-S, Nishihara H & Higuchi Y Structural basis for a [4Fe-3S] cluster in the oxygen-tolerant membrane-bound [NiFe]-hydrogenase. Nature 479, 253–256 (2011). [PubMed: 22002607]
14. Berkovitch F, Nicolet Y, Wan JT, Jarrett JT & Drennan CL Crystal structure of biotin synthase, an S-adenosylmethionine-dependent radical enzyme. Science 303, 76–79 (2004). [PubMed: 14704425]
15. Yao W, Gurubasavaraj PM & Holland PL All-ferrous iron-sulfur clusters. Struct. Bonding 160, 1–37 (2014).
16. Sickerman NS, Tanifuji K, Lee CC, Ohki Y, Tatsumi K, Ribbe MW & Hu Y Reduction of C1 substrates to hydrocarbons by the homometallic precursor and synthetic mimic of the nitrogenase cofactor. J. Am. Chem. Soc 139, 603–606 (2017). [PubMed: 28043123]
17. Tanifuji K, Sickerman N, Lee CC, Nagasawa T, Miyazaki K, Ohki Y, Tatsumi K, Hu Y & Ribbe MW Structure and reactivity of an asymmetric synthetic mimic of nitrogenase cofactor. Angew. Chem. Int. Ed 55, 15633–15636 (2016).
18. Tard C et al. Synthesis of the H-cluster framework of iron-only hydrogenase. Nature 433, 610–613 (2005). [PubMed: 15703741]
19. Holland PL Electronic structure and reactivity of three-coordinate iron complexes. Acc. Chem. Res 41, 905–914 (2008). [PubMed: 18646779]

20. Hoffman BM, Lukoyanov D, Yang Z-Y, Dean DR & Seefeldt LC Mechanism of nitrogen fixation by nitrogenase: the next stage. Chem. Rev 114, 4041–4062 (2014). [PubMed: 24467365]
21. Lancaster KM, Roemelt M, Ettenhuber P, Hu Y, Ribbe MW, Neese F, Bergmann U & DeBeer S X-ray emission spectroscopy evidences a central carbon in the nitrogenase iron-molybdenum cofactor. Science 334, 974–977 (2011). [PubMed: 22096198]
22. Spatzal T, Aksoyoglu M, Zhang L, Andrade SLA, Schleicher E, Weber S, Rees DC & Einsle O Evidence for interstitial carbon in nitrogenase FeMo cofactor. Science 334, 940–940 (2011). [PubMed: 22096190]
23. Spatzal T, Perez KA, Einsle O, Howard JB & Rees DC Ligand binding to the FeMo-cofactor: structures of CO-bound and reactivated nitrogenase. Science 345, 1620–1623 (2014). [PubMed: 25258081]
24. Sippel D et al. A bound reaction intermediate sheds light on the mechanism of nitrogenase. Science 359, 1484–1489 (2018). [PubMed: 29599235]
25. Vela J, Stoian S, Flaschenriem CJ, Münck E & Holland PL A sulfido-bridged diiron(II) compound and its reactions with nitrogenase-relevant substrates. J. Am. Chem. Soc 126, 4522–4523 (2004). [PubMed: 15070362]
26. Rodriguez MM, Stubbert BD, Scarborough CC, Brennessel WW, Bill E & Holland PL Isolation and characterization of stable iron(I) sulfide complexes. Angew. Chem. Int. Ed 51, 8247–8250 (2012).
27. MacLeod KC, Vinyard DJ & Holland PL A multi-iron system capable of rapid N2 formation and N2 cleavage. J. Am. Chem. Soc 136, 10226–10229 (2014). [PubMed: 25004280]
28. Strop P, Takahara PM, Chiu H-J, Angove HC, Burgess BK & Rees DC Crystal structure of the all-ferrous [4Fe-4S]0 form of the nitrogenase iron protein from azotobacter vinelandii. Biochemistry 40, 651–656 (2001). [PubMed: 11170381]
29. Tsou C-C, Lin Z-S, Lu T-T & Liaw W-F Transformation of dinitrosyl iron complexes [(NO)2Fe(SR)2]− (R = Et, Ph) into [4Fe-4S] clusters [Fe4S4(SPh)4]2−: relevance to the repair of the nitric oxide-modified ferredoxin [4Fe-4S] clusters. J. Am. Chem. Soc 130, 17154–17160 (2008). [PubMed: 19053409]
30. Ting-Wah Chu C, Yip-Kwai Lo F & Dahl LF Synthesis and stereochemical analysis of the [Fe4(NO)4(μ3-S)4]n series (n = 0, −1) which possesses a cubanelike Fe4S4 core: direct evidence for the antibonding tetrametal character of the unpaired electron upon a one-electron reduction of a completely bonding tetrahedral metal cluster. J. Am. Chem. Soc 104, 3409–3422 (1982).
31. Groom CR, Bruno IJ, Lightfoot MP Ward SC in Acta Crystallogr., Sect. B: Struct. Sci., Cryst. Eng. Mater Vol. 72 171–179 (2016).
32. Hagen KS, Watson AD & Holm RH Synthetic routes to iron sulfide (Fe2S2, Fe3S4, Fe4S4, and Fe6S9), clusters from the common precursor tetrakis(ethanethiolate)ferrate(2-) ion ([Fe(SC2H5)4]2-): structures and properties of [Fe3S4(SR)4]3- and bis(ethanethiolate)nonathioxohexaferrate(4-) ion ([Fe6S9(SC2H5)2]4-), examples of the newest types of Fe-S-SR clusters. J. Am. Chem. Soc 105, 3905–3913 (1983).
33. Osterloh F, Saak W, Pohl S, Kroeckel M, Meier C & Trautwein AX Synthesis and characterization of neutral hexanuclear iron sulfur clusters containing stair-like [Fe6(μ3-S)4(μ2-SR)4] and nest-like [Fe6(μ3-S)2(μ2-S)2(μ4-S)(μ2-SR)4] core structures. Inorg. Chem 37, 3581–3587 (1998). [PubMed: 11670447]
34. MacDonnell FM, Ruhlandt-Senge K, Ellison JJ, Holm RH & Power PP Sterically encumbered iron(II) thiolate complexes: synthesis and structure of trigonal planar [Fe(SR)3]- (R = 2,4,6-t-Bu3C6H2) and Mössbauer spectra of two- and three-coordinate complexes. Inorg. Chem 34, 1815–1822 (1995).
35. Yang L, Powell DR & Houser RP Structural variation in copper(I) complexes with pyridylmethylamide ligands: structural analysis with a new four-coordinate geometry index, τ4. Dalton Trans., 955–964 (2007). [PubMed: 17308676]
36. Angove HC, Yoo SJ, Burgess BK & Münck E Mössbauer and EPR evidence for an all-ferrous Fe4S4 cluster with S = 4 in the Fe protein of nitrogenase. J. Am. Chem. Soc 119, 8730–8731 (1997).

37. Leggate EJ, Bill E, Essigke T, Ullmann GM & Hirst J Formation and characterization of an all-ferrous Rieske cluster and stabilization of the [2Fe-2S]0 core by protonation. Proc. Natl. Acad. Sci. USA 101, 10913–10918 (2004). [PubMed: 15263097]
38. Gütlich PB, Eckhard; Trautwein AX Mossbauer spectroscopy and transition metal chemistry: fundamentals and applications. (Springer-Verlag, 2011).
39. Atanasov M, G. D, Sivalingam K, Neese F in Molecular Electronic Structures of Transition Metal Complexes II Vol. 143 (Springer, Berlin, 2011).
40. Gebhard MS, Koch SA, Millar M, Devlin FJ, Stephens PJ & Solomon EI Single-crystal spectroscopic studies of Fe(SR)42- (R = 2-(Ph)C6H4): electronic structure of the ferrous site in rubredoxin. J. Am. Chem. Soc 113, 1640–1649 (1991).
41. Figgis BN & Hitchman MA Ligand field theory and its applications. (Wiley-VCH, 2000).
42. Anderson JS & Peters JC Low-spin pseudotetrahedral iron(I) sites in Fe2(μ-S) complexes. Angew. Chem. Int. Ed 53, 5978–5981 (2014).
43. Carpino LA, Padykula RE, Barr DE, Hall FH, Krause JG, Dufresne RF & Thoman CJ Synthesis, characterization, and thermolysis of 7-amino-7-azabenzonorbornadienes. J. Org. Chem 53, 2565–2572 (1988).
44. Fox DJ & Bergman RG Synthesis of a first-row transition metal parent amido complex and carbon monoxide insertion into the amide N−H bond. J. Am. Chem. Soc 125, 8984–8985 (2003). [PubMed: 15369333]
45. Anderson JS, Moret M-E & Peters JC Conversion of Fe–NH2 to Fe–N2 with release of NH3. J. Am. Chem. Soc 135, 534–537 (2013). [PubMed: 23259776]
46. Creutz SEP, Jonas C Exploring secondary-sphere interactions in Fe–NxHy complexes relevant to N2 fixation. 8, 2321–2328 (2017).
47. Kiernicki JJ, Zeller M & Szymczak NK Hydrazine capture and N–N bond cleavage at iron enabled by flexible appended Lewis acids. J. Am. Chem. Soc 139, 18194–18197 (2017). [PubMed: 29227655]
48. Goh C, Weigel JA & Holm RH The [2:2] site-differentiated clusters [Fe4S4L2(RNC)6] containing two low-spin iron(II) sites. Inorg. Chem 33, 4861–4868 (1994).
49. Doan PE, Telser J, Barney BM, Igarashi RY, Dean DR, Seefeldt LC & Hoffman BM 57Fe ENDOR spectroscopy and ‘electron inventory’ analysis of the nitrogenase E4 intermediate suggest the metal-ion core of FeMo-cofactor cycles through only one redox couple. J. Am. Chem. Soc 133, 17329–17340 (2011). [PubMed: 21980917]
50. Barney BM, Yang T-C, Igarashi RY, Dos Santos PC, Laryukhin M, Lee H-I, Hoffman BM, Dean DR & Seefeldt LC Intermediates trapped during nitrogenase reduction of N⁝N, CH3−NNH, and H2N−NH2. J. Am. Chem. Soc 127, 14960–14961 (2005). [PubMed: 16248599]
51. Lukoyanov D, Dikanov SA, Yang Z-Y, Barney BM, Samoilova RI, Narasimhulu KV, Dean DR, Seefeldt LC & Hoffman BM ENDOR/HYSCORE studies of the common intermediate trapped during nitrogenase reduction of N2H2, CH3N2H, and N2H4 support an alternating reaction pathway for N2 reduction. J. Am. Chem. Soc 133, 11655–11664 (2011). [PubMed: 21744838]
52. Crossland JL & Tyler DR Iron–dinitrogen coordination chemistry: dinitrogen activation and reactivity. Coord. Chem. Rev 254, 1883–1894 (2010).
53. Rodriguez MM, Bill E, Brennessel WW & Holland PL N2 reduction and hydrogenation to ammonia by a molecular iron-potassium complex. Science 334, 780–783 (2011). [PubMed: 22076372]
54. Anderson JS, Rittle J & Peters JC Catalytic conversion of nitrogen to ammonia by an iron model complex. Nature 501, 84–87 (2013). [PubMed: 24005414]

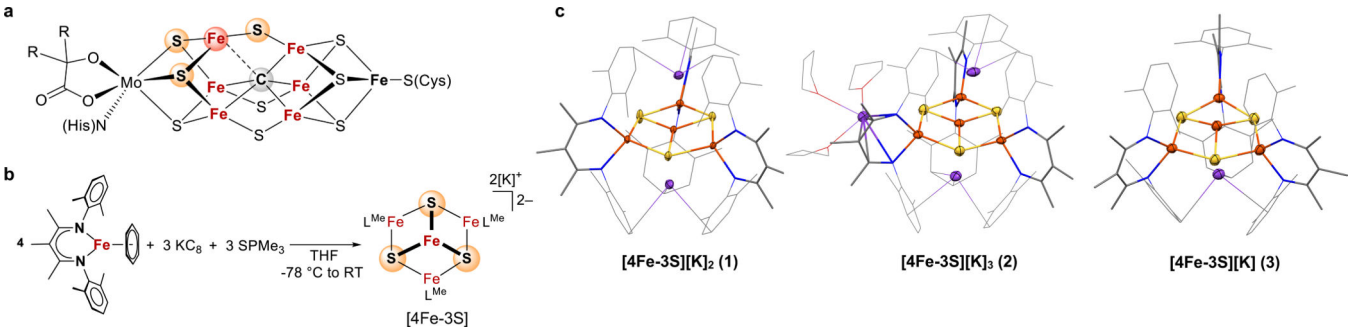

Figure 1. Preparation and relevance of a series of [4Fe-3S] clusters with trigonal planar iron.

a, Depiction of one hypothesis for how the FeMoco generates a substrate binding site through Fe-C bond cleavage to form three-coordinate iron sulfide; key atoms are highlighted with colored spheres. **b**, Synthetic route to three-coordinate iron-sulfur cluster [4Fe-3S], which features a three-coordinate iron sulfide site. **c**, Crystal structures of [4Fe-3S] clusters at three oxidation levels **1–3,** which demonstrate that the cluster core is retained across these oxidation levels.

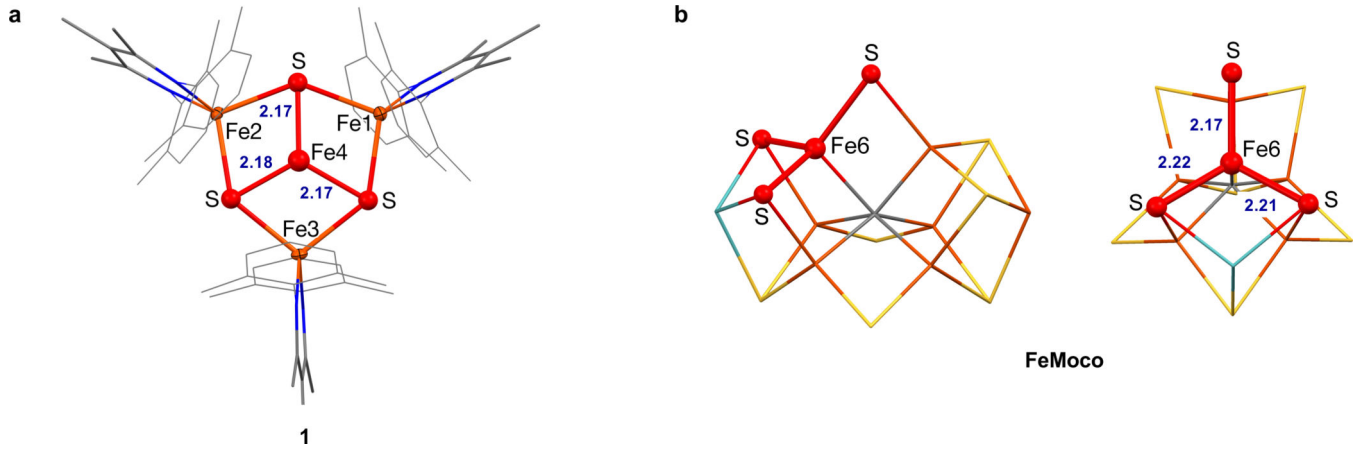

Figure 2. Structural analogy between [4Fe-3S] and the FeMoco.

In blue are the Fe–S bond distances at the three-coordinate iron of **1 (a)**, which are within error of those at the Fe6 site of the FeMoco[22] (**b**). In **b**, sulfur atoms are shown in yellow, molybdenum is in green, and carbon is in grey. The core of the [4Fe-3S] cluster—shown in red—is structurally similar to a proposed binding site in iron-sulfur clusters like the FeMoco, also highlighted in red.

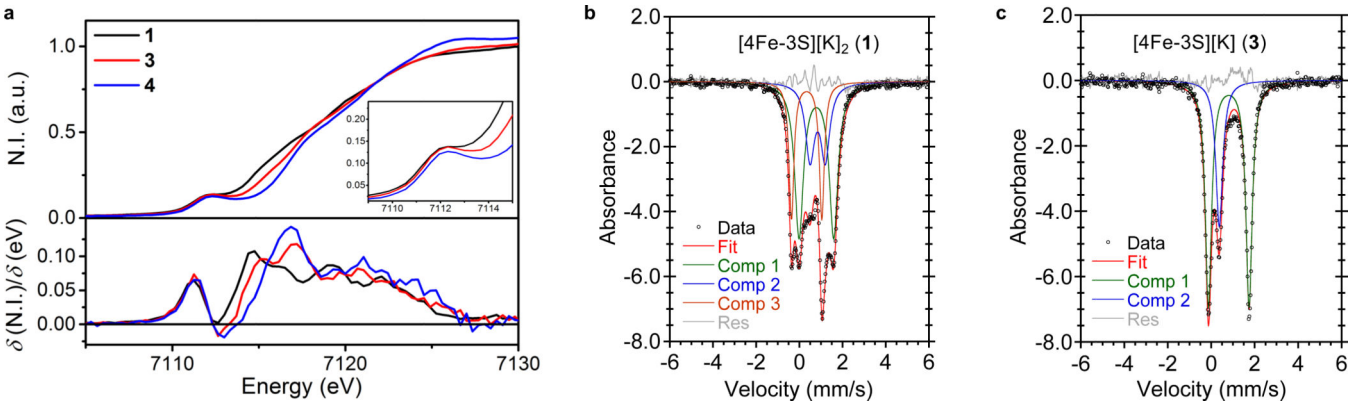

Figure 3. Spectroscopy of three-coordinate [4Fe-3S] clusters and amide coordinated product 4 gives insight into electronic structures.

a, Fe K-edge XAS spectra of [4Fe-3S] clusters [4Fe-3S][K]$_2$ (**1**), [4Fe-3S][K] (**3**), and [4Fe-3S][K]-NH$_2$ (**4**) (top) and the first derivatives (bottom). N.I. represents normalized intensity. These data indicate that metal-centered oxidation occurs at the central Fe site in going from reduced cluster **1** to oxidized cluster **3**. **b**, Mössbauer spectrum of **1** at 80 K, which shows three components in a 2:1:1 ratio for three high-spin Fe^{2+} sites and one central Fe^{1+} site. Component 1 (fixed at 50%, green): δ = 0.80 mm/s, | ΔE_Q| = 1.57 mm/s; Component 2 (fixed at 25%, blue): δ = 0.86 mm/s, | ΔE_Q| = 0.68 mm/s; Component 3 (fixed at 25%, orange) with δ = 0.34 mm/s, |ΔE_Q| = 1.38 mm/s. **c**, Mössbauer spectrum of **3** at 80 K, in which the minor component corresponds to an unusual low-spin Fe^{2+} site at the center of the cluster. Component 1 (75%, green): δ = 0.81 mm/s, |ΔE_Q| = 1.87 mm/s; Component 2 (25%, blue): δ = 0.37 mm/s, |ΔE_Q| = 0 mm/s.

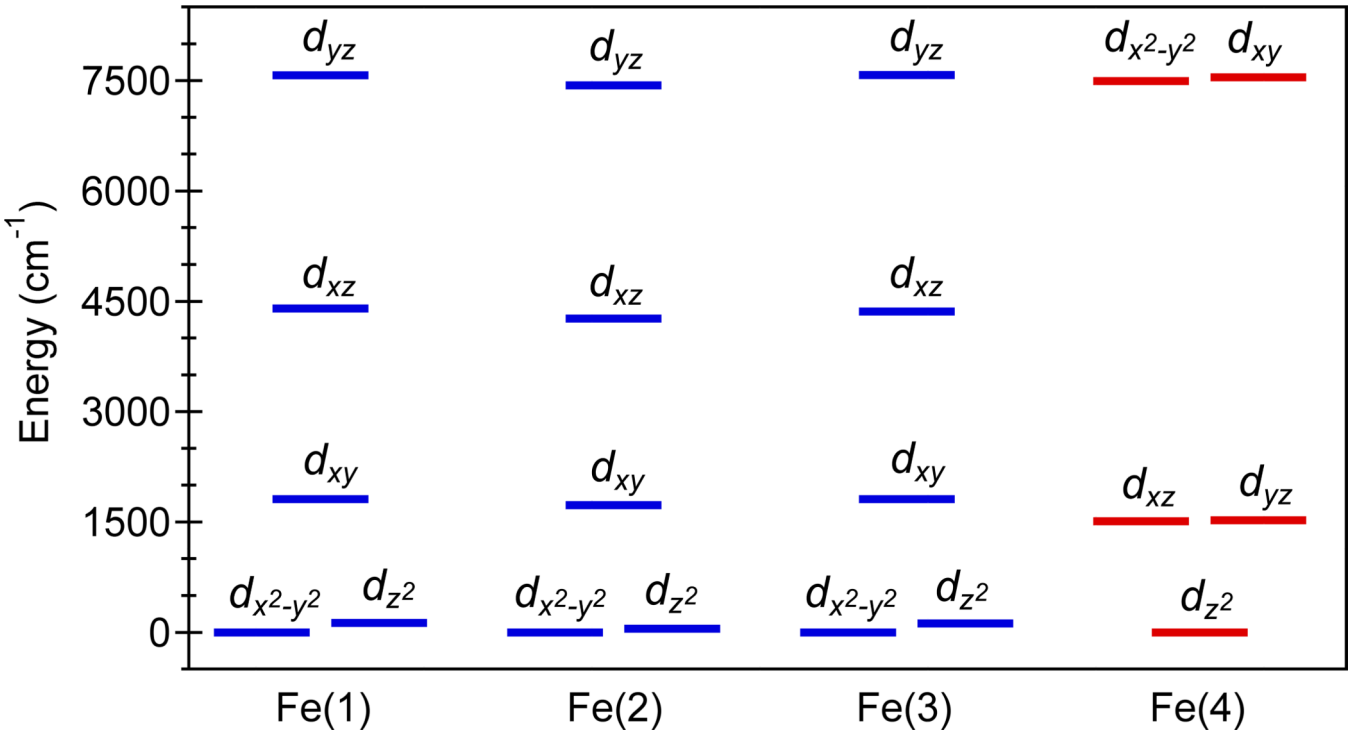

Figure 4. Calculated ligand field splitting diagram of iron sites in all-ferrous [4Fe-3S][K] (3).

Orbital energies were derived from AILFT on the basis of CASSCF/NEVPT2 calculations for models that isolate each iron site by replacing the other sites with closed-shell Zn^{2+}. The *z* axis is taken to be perpendicular to the Fe_4S_3 plane. The numbering of Fe sites corresponds to the X-ray crystal structure, and Fe4 is the central Fe site. The calculated ligand field splitting reveals that very short Fe–S bonds to the central Fe4 cause the d_{xy} and $d_{x2\text{-}y2}$ orbitals to be 6,000 cm^{-1} higher in energy than the next set of orbitals (d_{xz} and d_{yz}). This splitting is much larger than in typical tetrahedral sites of iron-sulfur clusters, and helps rationalize the low-spin configuration of the central Fe4 site.

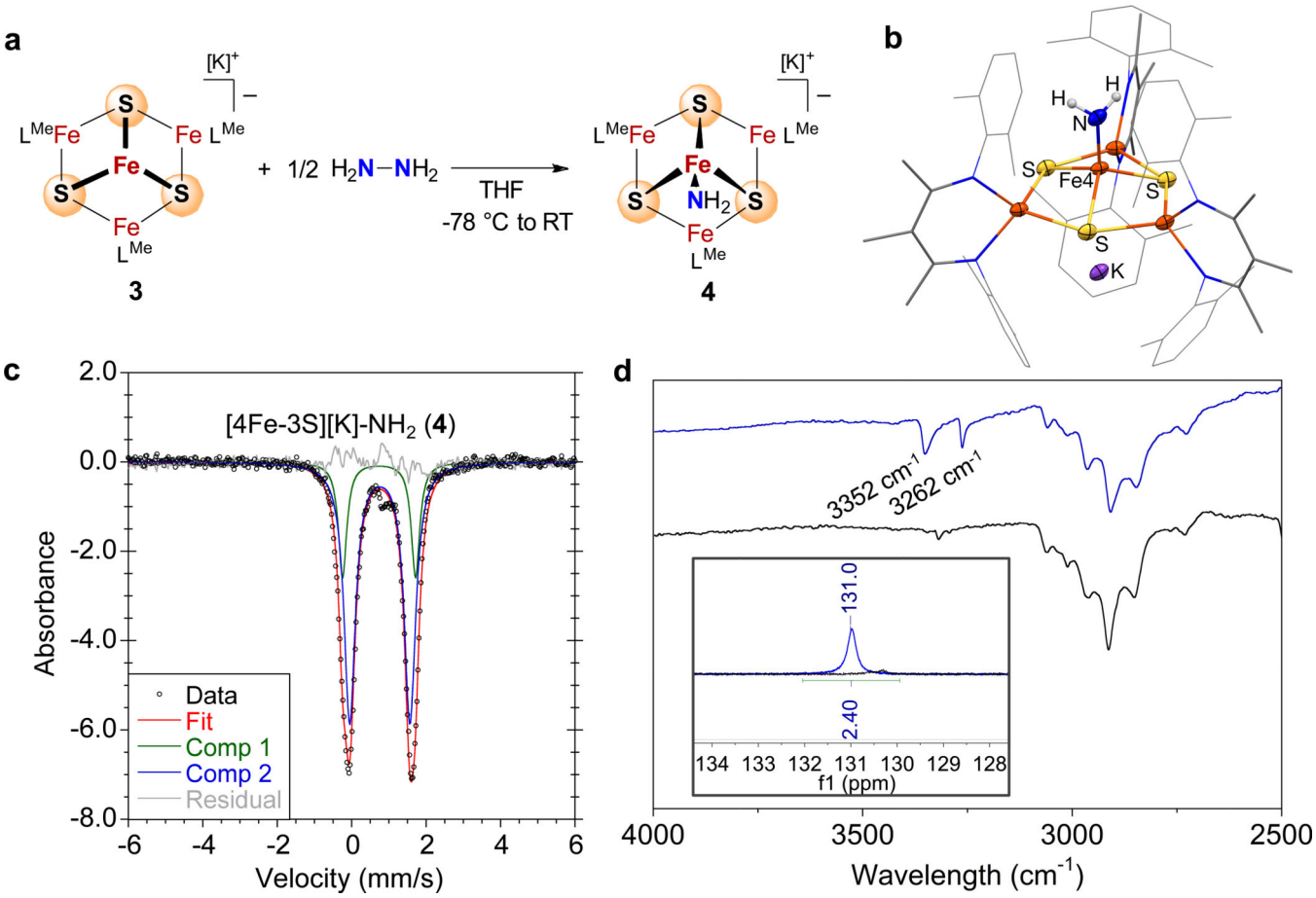

Figure 5. [4Fe-3S] reactivity with hydrazine and characterization of Fe–NH_2 product.

a, Reaction of all-ferrous [4Fe-3S] iron-sulfur cluster **3** with hydrazine, a nitrogenase substrate. **b**, Crystal structure of **4**, the resulting amide-coordinated [4Fe-3S] cluster. **c**, Mössbauer spectrum of **4** at 80 K. Component 1 (fixed at 25%, green): δ = 0.74 mm/s, $|\Delta E_Q|$ = 1.96 mm/s; Component 2 (fixed at 75%, blue): δ = 0.76 mm/s, $|\Delta E_Q|$ = 1.62 mm/s. **d**, Region of the IR spectrum of natural abundance **4** (blue trace) and deuterated **4** (black trace). Inset: ^{1}H NMR spectrum of **4** showing NH_2 protons (blue trace) overlaid with the spectrum of deuterated **4** (black trace) in which amide protons are not observed. These spectroscopic data identify the product of hydrazine reduction by all-ferrous **3** as an iron amide (Fe–NH_2). Full spectra are shown in Supplementary Figures 20, 26, and 33.